Research Article | Vol. 26, No. 19 | 17 Sep 2018 | OPTICS EXPRESS 24835
Optics EXPRESS

# Polarization-independent metasurface lens employing the Pancharatnam-Berry phase

DIANMIN LIN,[1,2] AARON L. HOLSTEEN,[1] ELHANAN MAGUID,[3] PENGYU FAN,[1] PIETER G. KIK,[1,4] EREZ HASMAN,[3] AND MARK L. BRONGERSMA[1,*]

[1]*Geballe Laboratory for Advanced Materials, Stanford University, Stanford, California 94305, USA*
[2]*Department of Electrical Engineering, Stanford University, Stanford, California 94305, USA*
[3]*Micro and Nanooptics Laboratory, Faculty of Mechanical Engineering and Russell Berrie Nanotechnology Institute, Technion–Israel Institute of Technology, Haifa 3200003, Israel*
[4]*CREOL, The College of Optics and Photonics, University of Central Florida, Florida 32816, USA*
**brongersma@stanford.edu*

**Abstract:** Metasurface optical elements, optical phased arrays constructed from a dense arrangement of nanoscale antennas, are promising candidates for the next generation of flat optical components. Metasurfaces that rely on the Pancharatnam-Berry phase facilitate complete and efficient wavefront control. However, their operation typically requires control over the polarization state of the incident light to achieve a desired optical function. Here, we circumvent this inherent sensitivity to the incident polarization by multiplexing two metasurfaces that were designed to achieve the same optical function with incident light of opposite helicity. We analyze the optical performance of different multiplexing approaches, and demonstrate a subwavelength random interleaved polarization-independent metasurface lens operating in the visible spectrum, providing a diffraction-limited spot size for the shared-aperture.



**OCIS codes:** (350.1370) Berry's phase; (160.3918) Metamaterials; (050.6624) Subwavelength structures.

## References and links

1. A. I. Kuznetsov, A. E. Miroshnichenko, M. L. Brongersma, Y. S. Kivshar, and B. Luk'yanchuk, "Optically Resonant Dielectric Nanostructures," Science **354**(6314), 6314 (2016).
2. L. Cao, J. S. White, J. S. Park, J. A. Schuller, B. M. Clemens, and M. L. Brongersma, "Engineering light absorption in semiconductor nanowire devices," Nat. Mater. **8**(8), 643–647 (2009).
3. A. B. Evlyukhin, C. Reinhardt, A. Seidel, B. S. Luk'yanchuk, and B. N. Chichkov, "Optical Response Features of Si-Nanoparticle Arrays," Phys. Rev. **82**(4), 45404B (2010).
4. L. Cao, P. Fan, E. S. Barnard, A. M. Brown, and M. L. Brongersma, "Tuning the Color of Silicon Nanostructures," Nano Lett. **10**(7), 2649–2654 (2010).
5. A. García-Etxarri, R. Gómez-Medina, L. S. Froufe-Pérez, C. López, L. Chantada, F. Scheffold, J. Aizpurua, M. Nieto-Vesperinas, and J. J. Sáenz, "Strong Magnetic Response of Submicron Silicon Particles in the Infrared," Opt. Express **19**(6), 4815–4826 (2011).
6. A. I. Kuznetsov, A. E. Miroshnichenko, Y. H. Fu, J. Zhang, and B. Luk'yanchuk, "Magnetic Light," Sci. Rep. **2**(1), 492 (2012).
7. Z. Bomzon, V. Kleiner, and E. Hasman, "Pancharatnam--Berry phase in space-variant polarization-state manipulations with subwavelength gratings," Opt. Lett. **26**(18), 1424–1426 (2001).
8. Z. Bomzon, G. Biener, V. Kleiner, and E. Hasman, "Space-variant Pancharatnam-Berry phase optical elements with computer-generated subwavelength gratings," Opt. Lett. **27**(13), 1141–1143 (2002).
9. P. Lalanne, S. Astilean, P. Chavel, E. Cambril, and H. Launois, "Blazed binary subwavelength gratings with efficiencies larger than those of conventional échelette gratings," Opt. Lett. **23**(14), 1081–1083 (1998).
10. P. Lalanne, S. Astilean, P. Chavel, E. Cambril, and H. Launois, "Design and Fabrication of Blazed Binary Diffractive Elements with Sampling Periods Smaller than the Structural Cutoff," J. Opt. Soc. Am. A **16**(5), 1143–1156 (1999).
11. N. Yu, P. Genevet, M. A. Kats, F. Aieta, J. P. Tetienne, F. Capasso, and Z. Gaburro, "Light Propagation with Phase Discontinuities: Generalized Laws of Reflection and Refraction," Science **334**(6054), 333–337 (2011).
12. D. Lin, P. Fan, E. Hasman, and M. L. Brongersma, "Dielectric gradient metasurface optical elements," Science **345**(6194), 298–302 (2014).
13. P. Lalanne and P. Chavel, "Metalenses at visible Wavelengths Past, Present, Perspectives," Laser Photonics Rev. **11**(3), 1600295 (2017).

#331968 https://doi.org/10.1364/OE.26.024835
Journal © 2018 Received 14 Jun 2018; revised 22 Jul 2018; accepted 22 Jul 2018; published 10 Sep 2018

Optics EXPRESS


14. A. V. Kildishev, A. Boltasseva, and V. M. Shalaev, "Planar Photonics with Metasurfaces," Science **339**(6125), 1232009 (2013).
15. A. Pors, O. Albrektsen, I. P. Radko, and S. I. Bozhevolnyi, "Gap plasmon-based metasurfaces for total control of reflected light," Sci. Rep. **3**(1), 2155 (2013).
16. M. I. Shalaev, J. Sun, A. Tsukernik, A. Pandey, K. Nikolskiy, and N. M. Litchinitser, "High-Efficiency All-Dielectric Metasurfaces for Ultracompact Beam Manipulation in Transmission Mode," Nano Lett. **15**(9), 6261–6266 (2015).
17. E. Hasman, V. Kleiner, G. Biener, and A. Niv, "Polarization Dependent Focusing Lens by Use of Quantized Pancharatnam-Berry Phase Diffractive Optics," Appl. Phys. Lett. **82**(3), 328–330 (2003).
18. D. Fattal, J. J. Li, Z. Peng, M. Fiorentino, and R. G. Beausoleil, "Flat Dielectric Grating Reflectors with Focusing Abilities," Nat. Photonics **4**(7), 466–470 (2010).
19. A. Arbabi, Y. Horie, A. J. Ball, M. Bagheri, and A. Faraon, "Subwavelength-Thick Lenses with High Numerical Apertures and Large Efficiency Based on High-Contrast Transmitarrays," Nat. Commun. **6**(1), 7069 (2015).
20. K. Zhang, Y. Yuan, D. Zhang, X. Ding, B. Ratni, S. N. Burokur, M. Lu, K. Tang, and Q. Wu, "Phase-engineered metalenses to generate converging and non-diffractive vortex beam carrying orbital angular momentum in microwave region," Opt. Express **26**(2), 1351–1360 (2018).
21. X. Ni, A. V. Kildishev, and V. M. Shalaev, "Metasurface Holograms for Visible Light," Nat. Commun. **4**(1), 2807 (2013).
22. X. Chen, L. Huang, H. Mühlenbernd, G. Li, B. Bai, Q. Tan, G. Jin, C. W. Qiu, S. Zhang, and T. Zentgraf, "Dual-Polarity Plasmonic Metalens for Visible Light," Nat. Commun. **3**(1), 1198 (2012).
23. N. Dahan, Y. Gorodetski, K. Frischwasser, V. Kleiner, and E. Hasman, "Geometric Doppler Effect: Spin-Split Dispersion of Thermal Radiation," Phys. Rev. Lett. **105**(13), 136402 (2010).
24. N. Shitrit, I. Yulevich, E. Maguid, D. Ozeri, D. Veksler, V. Kleiner, and E. Hasman, "Spin-Optical Metamaterial Route to Spin-Controlled Photonics," Science **340**(6133), 724–726 (2013).
25. N. Shitrit, I. Bretner, Y. Gorodetski, V. Kleiner, and E. Hasman, "Optical Spin Hall Effects in Plasmonic Chains," Nano Lett. **11**(5), 2038–2042 (2011).
26. X. Yin, Z. Ye, J. Rho, Y. Wang, and X. Zhang, "Photonic Spin Hall Effect at Metasurfaces," Science **339**(6126), 1405–1407 (2013).
27. S. Vo, D. Fattal, W. V. Sorin, Z. Peng, T. Tran, M. Fiorentino, and R. G. Beausoleil, "Sub-wavelength grating lenses with a twist," IEEE Photonics Technol. Lett. **26**(13), 1375–1378 (2014).
28. Y. F. Yu, A. Y. Zhu, R. Paniagua-Domínguez, Y. H. Fu, B. Luk'yanchuk, and A. I. Kuznetsov, "High-Transmission Dielectric Metasurface with 2π Phase Control at Visible Wavelengths," Laser Photonics Rev. **9**(4), 412–418 (2015).
29. E. Arbabi, A. Arbabi, S. M. Kamali, Y. Horie, and A. Faraon, "Multiwavelength Polarization-Insensitive Lenses Based on Dielectric Metasurfaces with Meta-Molecules," Optica **3**(6), 628–633 (2016).
30. Q.-T. Li, F. Dong, B. Wang, F. Gan, J. Chen, Z. Song, L. Xu, W. Chu, Y. F. Xiao, Q. Gong, and Y. Li, "Polarization-Independent and High-Efficiency Dielectric Metasurfaces for Visible Light," Opt. Express **24**(15), 16309–16319 (2016).
31. M. Khorasaninejad, A. Y. Zhu, C. Roques-Carmes, W. T. Chen, J. Oh, I. Mishra, R. C. Devlin, and F. Capasso, "Polarization-Insensitive Metalenses at Visible Wavelengths," Nano Lett. **16**(11), 7229–7234 (2016).
32. B. Y. S. Pancharatnam, "Generalized Theory of Interference and Its Applications-I," Proc. Indiana Acad. Sci. **44**(4), 247–262 (1956).
33. M. V. Berry, "Quantal Phase Factors Accompanying Adiabatic Changes," in *Proceedings of the Royal Society of London A: Mathematical, Physical and Engineering Sciences* (1984), pp. 45–57.
34. M. Khorasaninejad, W. T. Chen, R. C. Devlin, J. Oh, A. Y. Zhu, and F. Capasso, "Metalenses at visible wavelengths: Diffraction-limited focusing and subwavelength resolution imaging," Science **352**(6290), 1190–1194 (2016).
35. M. Khorasaninejad, W. T. Chen, A. Y. Zhu, J. Oh, R. C. Devlin, D. Rousso, and F. Capasso, "Multispectral Chiral Imaging with a Metalens," Nano Lett. **16**(7), 4595–4600 (2016).
36. Y. Gorodetski, G. Biener, A. Niv, V. Kleiner, and E. Hasman, "Space-variant polarization manipulation for far-field polarimetry by use of subwavelength dielectric gratings," Opt. Lett. **30**(17), 2245–2247 (2005).
37. A. Pors, M. G. Nielsen, and S. I. Bozhevolnyi, "Plasmonic metagratings for simultaneous determination of Stokes parameters," Optica **2**(8), 716 (2015).
38. J. P. Balthasar Mueller, K. Leosson, and F. Capasso, "Ultracompact metasurface in-line polarimeter," Optica **3**(1), 42 (2016).
39. D. M. Pozar and S. D. Targonski, "A shared-aperture dual-band dual-polarized microstrip array," IEEE Trans. Antenn. Propag. **49**(2), 150–157 (2001).
40. R. L. Haupt, "Interleaved thinned linear arrays," IEEE Trans. Antenn. Propag. **53**(9), 2858–2864 (2005).
41. A. M. Sayeed and V. Raghavan, "Maximizing MIMO capacity in sparse multipath with reconfigurable antenna arrays," IEEE J. Sel. Top. Signal Process. **1**(1), 156–166 (2007).
42. M. LeCompte, S. Y. Shi, and D. W. Prather, ""Interleaved diffractive optical element design," Wave-Optical," Syst. Eng. **4436**, 115–122 (2001).
43. D. Lin, A. L. Holsteen, E. Maguid, G. Wetzstein, P. G. Kik, E. Hasman, and M. L. Brongersma, "Photonic Multitasking Interleaved Si Nanoantenna Phased Array," Nano Lett. **16**(12), 7671–7676 (2016).

Optics EXPRESS

44. E. Maguid, I. Yulevich, D. Veksler, V. Kleiner, M. L. Brongersma, and E. Hasman, "Photonic spin-controlled multifunctional shared-aperture antenna array," Science **352**(6290), 1202–1206 (2016).
45. E. Maguid, I. Yulevich, M. Yannai, V. Kleiner, M. L. Brongersma, and E. Hasman, "Multifunctional Interleaved Geometric-Phase Dielectric Metasurfaces," Light Sci. Appl. **6**(8), e17027 (2017).
46. E. Hasman, N. Davidson, and A. A. Friesem, "Efficient Multilevel Phase Holograms for CO2 Lasers," Opt. Lett. **16**(6), 423–425 (1991).

## 1. Introduction

Dielectric optical nanoantennas are well-known for their ability to manipulate light at a sub-wavelength scale [1–6]. Flat optical components can be constructed from a dense arrangement of such structures in a planar arrangement and operate in a similar fashion to phased array antennas capable of reshaping the wavefront of an incident light wave [7–13]. These optical components are often called metasurfaces to emphasize that they are thin compared to the free-space wavelength of light [14]. They have enabled the realization of a range of optical functions and new physical concepts, including beam steering [9, 10, 15, 16], lenses [17–20], holograms [21, 22], thermal radiation control components [23], the optical Rashba effect [23, 24] and spin-optical devices [25, 26].

One type of metasurface is composed of antennas whose size or shape varies with position. A practical advantage of such components is that their operation can easily be rendered insensitive to the polarization state of the incident light [9, 15, 19, 27–31]. However, their phase profile tends to produce a highly dispersive performance, and it is challenging to decouple the local transmissivity and phase response as both have distinct dependencies on the antenna size and shape. The second type is based on the Pancharatnam-Berry phase (geometric phase) [32, 33] that results from a space-variant orientation of optical nano-antennas in order to control the local phase pick-up [7, 8, 12, 17, 34]. The geometric phase emerging from a surface patterned with such oriented nano-antennas is given by $\phi_g = 2\sigma\theta(x, y)$, where $\sigma = \pm 1$ denotes the incident polarization helicity photonic spin-states, right ($\sigma_+$) and left ($\sigma_-$) circular polarization; here $\theta(x, y)$ is the orientation profile. Importantly, this phase can be designed to span the full $2\pi$ range while maintaining uniform transmission amplitude, resulting in high diffraction efficiencies across broad operational bandwidths. However, achieving a desired optical function using geometric phase typically requires the use of circularly-polarized light, and distinct optical properties are obtained for incident light beams with opposing helicities. For example, a metasurface designed to focus incident light with right circular polarization, will diverge for incident left circular polarization [7, 8, 17]. This distinct response offered by such a metasurface has been exploited for chiral imaging [35] and polarimetry [36–38].

Here, we propose a polarization-independent metasurface based on the Pancharatnam-Berry phase and shared-aperture phased-array concepts [39–45]. The polarization independence results from spatial multiplexing of two metasurfaces that are designed to provide the same optical function for incident light beams of opposite helicity. Study of the spatial multiplexing technique together with the optical performance of the components is presented. In this work we demonstrate interleaved flat optical lenses that preserve the numerical aperture of the entire shared-aperture, and that offer a polarization-independent focusing of the incident light using an ultrathin lightweight optical element.

## 2. Polarization-independent lens based on the geometric phase

Figure 1 illustrates the design principle of a polarization-independent flat lens utilizing the geometric phase. Previously, it was demonstrated that a spherical geometric phase metasurface focuses light into a diffraction-limited focal spot in a spin-dependent manner (see Fig. 1(a) and 1(e)) [12, 17]. First a 90-μm-diameter lens with a focal length $f$ of 100 μm is designed to focus an incident $\sigma_-$ beam at wavelength $\lambda$ of 550 nm. A calculation based on the Fresnel approximation shows a diffraction limited focal spot with a 0.75 μm full width at half maximum (FWHM), however incident light of opposite spin will be defocused.

Optics EXPRESS

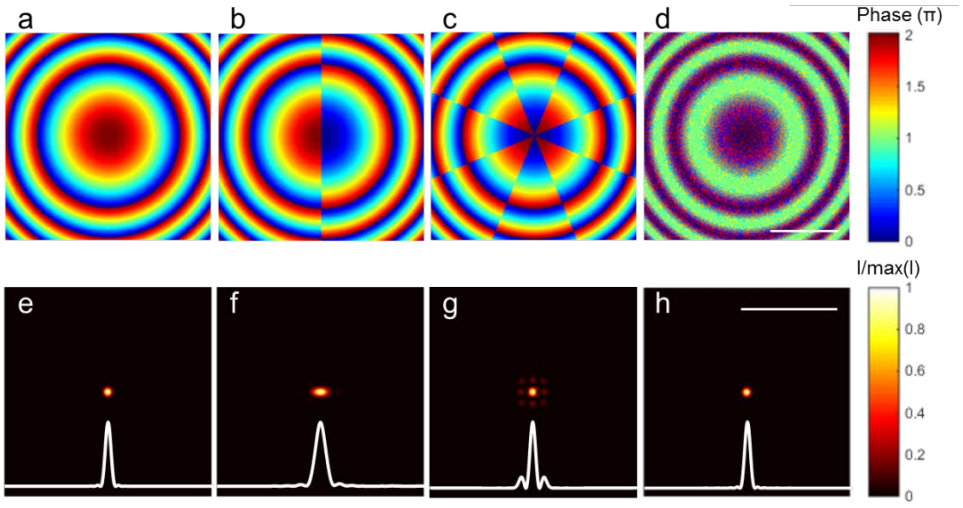


Fig. 1. Calculated phase profiles and diffraction patterns for single and spatially multiplexed flat optical lenses. The phase profiles are shown for $\sigma_-$ for (a) a single, 90-μm-diameter lens, (b) a multiplexed lens composed of 2-segments/half-lenses which feature reversed phase profiles to allow focusing of both $\sigma_-$ and $\sigma_+$, (c) a multiplexed lens composed of 8 segments, (d) a randomly interleaved lens. (e-h) The corresponding amplitude distributions for the calculated diffraction pattern at the focal plane under plane wave illumination with 550 nm circularly polarized light. The intensity distribution through the focus is shown in the inset. The amplitude is normalized to the maximum intensity for each focal spot. The length of the scale bar is 10 μm.

A simple approach to focus light of both circular polarizations is to divide the lens into two equally sized segments, with the left side the geometric mirror image of the right side. Hence, we assign a distinct orientation profile to each segment according to

$$2\theta_1(x,y) = \tfrac{2\pi}{\lambda}(f - \sqrt{x^2 + y^2 + f^2}),\ 2\theta_2(x,y) = -\tfrac{2\pi}{\lambda}(f - \sqrt{x^2 + y^2 + f^2}).$$

Each half-lens segment focuses light of a distinct helicity onto the focal plane. Together, the two halves form a new, segmented, 90-μm-diameter lens as depicted in Fig. 1b. The calculated focal spot is elongated along the horizontal direction due to the reduced aperture of each individual sub-lens in the horizontal direction (see Fig. 1(f)). The theoretically calculated FWHM from Fig. 1(f) is of 1.3 μm and 0.72 μm along the x and y directions, respectively. Another approach is given by a multiplexed lens that uses a larger number of segments, which can be accomplished for example by creating more tangential segments, as illustrated in Fig. 1(c). Figure 1(g) shows that the resulting focal spot is indeed reduced in size and assumes a more circular shape. However, due to the periodic tangential segments, a set of undesired diffraction spots around the central focus is obtained. To avoid this imaging artifact we further interleave these conjugated lenses through spatially randomized subwavelength multiplexing. The spatial interleaving is implemented by dividing each of the distinct phase profiles into equally distributed segments, then randomly selecting the segments from the multiple distinct phase profiles to produce random spatial multiplexing. The interleaved lens is constructed from numerous segments, and maintains the diffraction-limit of the shared aperture as depicted in Fig. 1(d) and 1(h), while suppressing undesired diffraction spots. From this analysis, it is clear that one can use the random interleaving approach to effectively incorporate the optical functionality of two distinct optical elements into one spatial surface area. Note the maximum intensity ($I_M$) of the focal spots in Figs. 1(f)-1(h) are 0.251 $I_0$, 0.252 $I_0$ and 0.260 $I_0$ respectively; where $I_0$ is the maximum intensity for a perfect full lens. The maximum intensity for the interleaved lens is in agreement with the theoretical prediction of

Optics EXPRESS

$1/N^2 = 0.25$, where the reduced energy in the focal spot is distributed to the side lobe or speckle noise. The integrated power at the focal plane in the case of Fig. 1(f)-1(h) is approximately reduced according to $1/N = 1/2$, where $N$ is the number of channels by which light is focused. This is in correlation to the effective aperture of each phase profile [43, 44]. Segmented polarization-independent lens based on geometric phase preserves the advantages of geometric phase based optical element and gives rise to additional optical functionalities, but with a reduction in it intensity.

The phase profiles are implemented with 8-discrete levels [46] using poly-crystalline Si nanobeam antennas with subwavelength spacings and space-varying orientations [12]. The antennas are 100 nm high, 120 nm wide and feature an edge-to-edge-spacing of 80 nm. We experimentally investigate the focusing performance of the lens with 2-segments first and fabricate it by electron-beam lithography (see Fig. 2(a)). To analyze the optical performance of the lens we illuminate the structure with a collimated circularly-polarized beam, at a wavelength of 550 nm from a spectrally filtered supercontinuum laser. The detail of the fabrication procedure and optical characterization can be found in our previous publication [12]. Figures 2(b) and 2(c) demonstrate the intensity distribution in the focal plane which was measured using a confocal microscope, where the FWHM of the focal spot is 1.44 μm and 0.765 μm along the x and y directions, respectively. These results are in good agreement with the theory shown in Fig. 1f. The size and shape of the focal spot at the focal plane are identical to those obtained with circularly-polarized light, demonstrating the polarization-independent performance. However, the focused light is seen to be tilted away from the optical axis and also characterized by a large FWHM along the x-direction due to the fact that only half of the metasurface lens contributes to the focus for a given circular polarization. When the lens is illuminated with linearly-polarized light, constituted from equal amounts of $\sigma_-$ and $\sigma_+$, it focuses this light onto the designed focal plane in a slightly different fashion along propagation axis (see Figs. 2(d) and 2(e)).

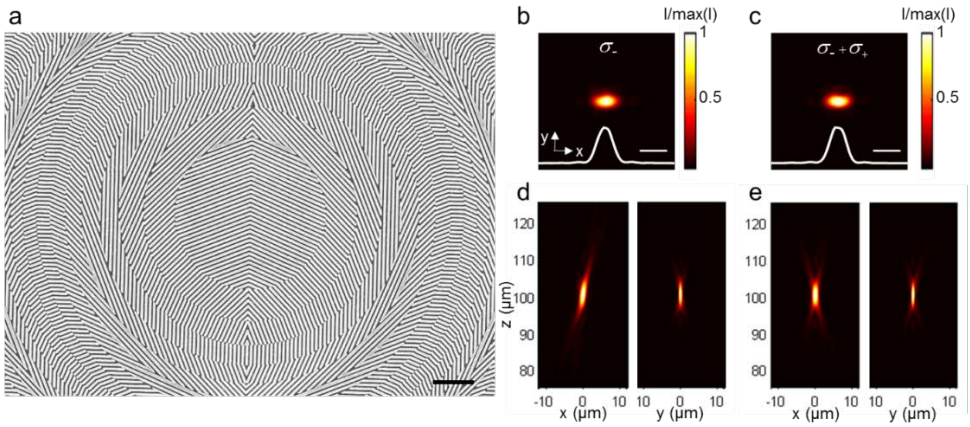


Fig. 2. (a) Scanning electron microscope image of a metasurface lens composed of 2 segments. (b and c) Measured intensity profile of the focal spot in the focal plane at z = 100 μm upon illumination with left circularly (b) and linear (c) polarization. The inset shows the intensity distribution through the focus along the *x*-axis. (d and e) Measured intensity profile of the transmitted light behind the polarization-independent metasurface lens along x-z plane and y-z plane upon illumination with circularly (d) and linearly (e) polarized light. The scale bars in the panels are 2 μm.

## 3. Polarization-independent lenses with randomly interleaved antennas

We also studied the performance of polarization-independent lenses with randomly interleaved antennas. The design starts by establishing the required geometric phase profile for a single metasurface lens that effectively focuses $\sigma_-$ and $\sigma_+$, individually (see schematic in

Optics EXPRESS

Fig. 3). In order to achieve a rotationally symmetric performance, we divide concentric rings in the lens into a large number of segments and then randomly assigned the phase-profile of either the $\sigma_-$ or $\sigma_+$.

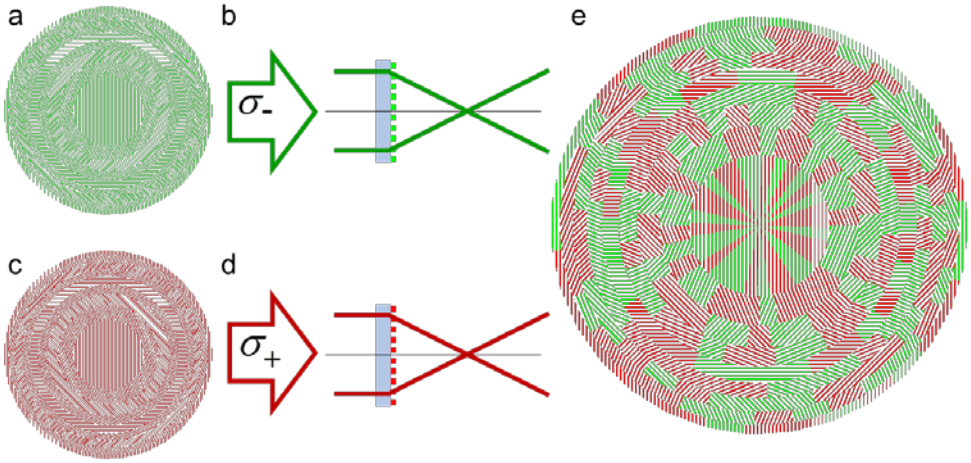


Fig. 3. Random subwavelength interleaved approach. (a-d) Nanopattern design for a single metasurface lens showing how incident $\sigma_-$ (a,b) and $\sigma_+$ (c,d) is focused by the metasurface lens. (e) Design of a polarization-independent interleaved metasurface lens. Concentric rings in the lens were divided up in segments and randomly assigned the phase-profile of either the $\sigma_+$ or $\sigma_-$

We fabricated the designed metasurface lens by electron-beam lithography as shown in Fig. 4(a), and illuminated it with a collimated 550 nm wavelength circular polarized beam as (see results in Figs. 4(b) and 4(c)). This demonstrates that both the spot size and the intensity distribution in the focal plane is the same for the two opposing helicities. A radially symmetric focal spot was measured with a FWHM of 0.85 μm, thanks to the larger effective aperture through random interleaving, which is in a good agreement with theory and much smaller than the focal spots shown in Fig. 2 **(**FWHM = 1.44 μm**)**. Importantly, when the random interleaved metasurface is illuminated with linearly polarized light, the measured focal spot is equal to the measured foci for $\sigma_-$ or $\sigma_+$ illumination individually as shown in Fig. 4(d). The measured optical intensity distributions of the transmitted beam along the propagation direction which are demonstrated in Figs. 4(e)-4(g), show that the intensity distributions of the focused beam along the optical axis are identical regardless of the polarization state of the incident light. The size and intensity of the measured focal spot fully agrees with the theoretical prediction, as discussed in Fig. 1h. This demonstrates that the interleaving approach allows the creation of a lens with a numerical aperture that corresponds to the shared-aperture. Note that this lens will work for unpolarized light – an incoherent superposition of $\sigma_+$ and $\sigma_-$.

Optics EXPRESS

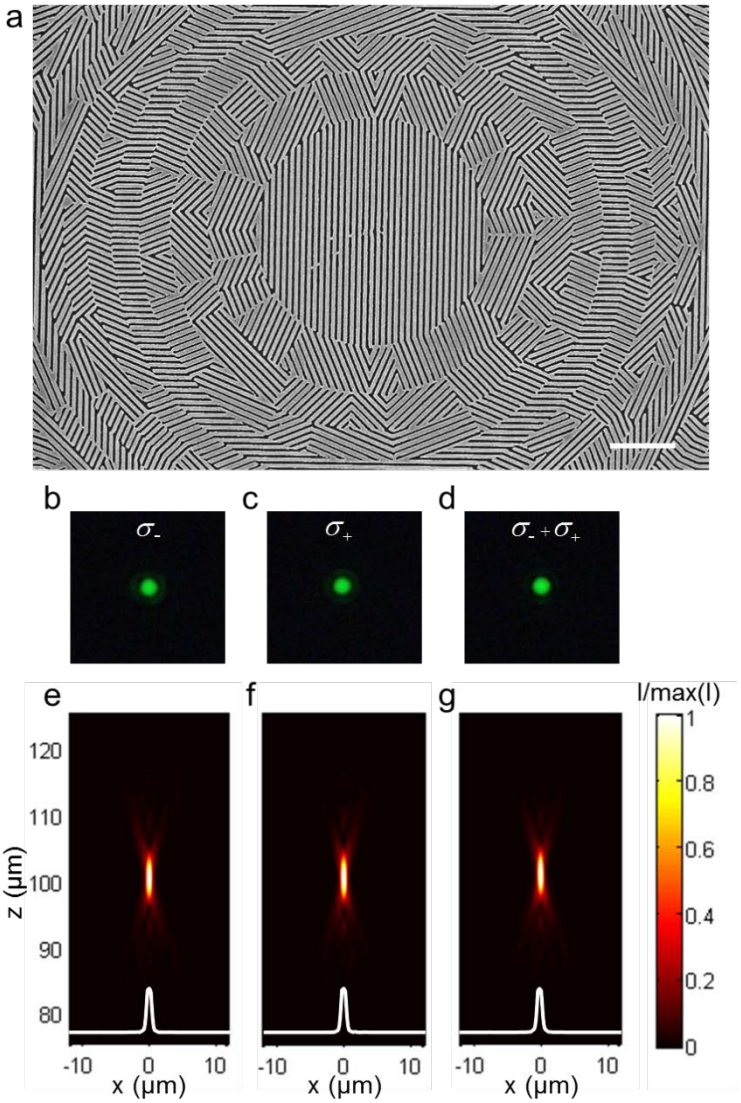


Fig. 4. (a) Scanning electron microscope image of the fabricated polarization-independent random interleaved metasurface lens. The scale bar is 2 μm. (b-d) Optical microscope images of the focal spot measured at a focal plane of z = 100 μm upon illumination with σ-, σ+ and linear polarization, respectively. (e-g) Measured intensity profile in the x-z plane upon illumination with σ-, σ+ and linear polarized light, respectively. The inset along the x-axis shows the cross-sectional intensity profile at the focal plane, z = 100 μm.

## 4. Concluding remarks

In conclusion, we have demonstrated polarization-independent metasurface lenses based on the geometric phase through a multiplexing approach. The elements are constructed from nanoscale Si antennas that afford operation in the visible spectral range. We investigated the optical properties of such metasurfaces with various degrees of multiplexing. The design approach, which was demonstrated for a lens, can be easily extended to polarization-independent metasurfaces that exhibit other optical functions. This further extends the possible use of geometric phase elements for a wide range of integrated optical applications in imaging and display.

Optics EXPRESS

## Funding

United States-Israel Binational Science Foundation (BSF); the Global Climate and Energy Project; U.S. Air Force Office for Science Research (FA9550-17-1-0331).

## Acknowledgments

We acknowledge funding support listed above. A.L.H. acknowledges support from an Air Force Office of Scientific Research, National Defense Science and Engineering Graduate (NDSEG) Fellowship, 32 CFR 168a.